New insights into triaxiality and shape coexistence from odd-mass ^{109}Rh

B. Bucher, H. Mach, A. Aprahamian, L. M. Robledo, G. S. Simpson, J. Rissanen, D. G. Ghiţă, B. Olaizola, W. Kurcewicz, J. Äystö, T. Eronen, L. M. Fraile, A. Jokinen, P. Karvonen, I. D. Moore, H. Penttilä, M. Reponen, E. Ruchowska, A. Saastamoinen, M. K. Smith, and C. Weber

Phys. Rev. C **98**, 064320 — Published 20 December 2018

DOI: 10.1103/PhysRevC.98.064320

New Insights on Triaxiality and Shape Coexistence from Odd-Mass ^{109}Rh

B. Bucher,[1,2,*] H. Mach,[2,3,†] A. Aprahamian,[2] L. M. Robledo,[4] G. S. Simpson,[5] J. Rissanen,[6,‡] D. G. Ghiţă,[7] B. Olaizola,[8,§] W. Kurcewicz,[9] J. Äystö,[6] T. Eronen,[6] L. M. Fraile,[8] A. Jokinen,[6] P. Karvonen,[6,¶] I. D. Moore,[6] H. Penttilä,[6] M. Reponen,[6] E. Ruchowska,[3] A. Saastamoinen,[6,**] M. K. Smith,[2,††] and C. Weber[6,‡‡]

[1] *Idaho National Laboratory, Idaho Falls, Idaho 83415 USA*
[2] *Department of Physics, University of Notre Dame, Notre Dame, Indiana 46556 USA*
[3] *Division of Nuclear Physics, BP1, National Centre for Nuclear Research, ul. Hoża 69, 00-681, Warsaw, Poland*
[4] *Departamento de Física Teórica, Universidad Autónoma de Madrid, E-28049 Madrid, Spain*
[5] *Univ. Grenoble Alpes, CNRS, Grenoble INP*, LPSC-IN2P3, 38000 Grenoble, France*
[6] *Department of Physics, University of Jyväskylä, P.O. Box 35, FI-40014 Jyväskylä, Finland*
[7] *National Institute for Physics and Nuclear Engineering, R-77125 Bucharest-Magurele, Romania*
[8] *Grupo de Física Nuclear e IPARCOS, Universidad Complutense de Madrid, CEI Moncloa, E-28040 Madrid, Spain*
[9] *Faculty of Physics, University of Warsaw, Pasteura 5, PL 02-093 Warsaw, Poland*

(Dated: November 26, 2018)

Rapid shape evolutions near A=100 are now the focus of much attention in nuclear science. Much of the recent work has been centered on isotopes with $Z\leq$40, where the shapes are observed to transition between near-spherical to highly-deformed with only a single pair of neutrons added. At higher Z, the shape transitions become more gradual as triaxiality sets in, yet the coexistence of varying shapes continues to play an important role in the low-energy nuclear structure, particularly in the odd-Z isotopes. This work aims to characterize competing shapes in the triaxial region between Zr and Sn isotopes using ultra-fast timing techniques to measure lifetimes of excited states in the neutron-rich nucleus, ^{109}Rh. The measurements confirm the persistence at higher-Z of similarly-large deformations observed near Z=40. Moreover, we show that new self-consistent mean-field calculations, with proper treatment of the odd nucleon, are able to reproduce the coexisting triaxial and highly-deformed configurations revealing, for the first time, the important contribution of the unpaired nucleon to these different shapes based on the blocking of specific single-particle orbitals.

PACS numbers: 29.30.Kv, 27.60.+j, 23.20.-g, 21.60.Jz, 21.10.Tg

I. INTRODUCTION

One of the overarching questions in nuclear physics today, as increasingly neutron-rich isotopes become more and more accessible, is concerned with how intrinsic nuclear shapes and their related shell structure evolve away from stability. There is now a wealth of evidence to indicate that the traditional magic numbers describing nuclear shell structure often do not hold for isotopes that sit off the valley of stability [1–8]. The mechanism driving the evolution of shell structure is generally attributed to various forms of residual interactions between the outermost valence nucleons [4–6, 9–12]. These residual interactions effectively alter the overall shape of the nuclear potential as more nucleons are added, thus modifying the underlying single-particle structure which can result in a quenching of shell gaps along with the creation of new gaps elsewhere.

One of the best examples of this phenomenon is seen in the region of neutron-rich nuclides with $A\sim$100 [11, 13–18]. In this region, near-spherical and highly quadrupole-deformed shapes are observed to closely compete for the lowest energy configuration resulting in wide shape variations between neighboring isotopes. As a result, these isotopes provide a sensitive test for modern nuclear models rooted in density functional theory (DFT) [19–25] or even large-scale Monte Carlo Shell Model (MCSM) calculations [26–28] that are both capable of predicting nuclear properties out to extreme neutron-to-proton ratios. Indeed, the rapidly varying nuclear structure in this region has recently been attributed to large-scale reconfiguration of single-particle orbitals near the Fermi surface, known as Type II shell evolution [26–28], however such calculations have so far been limited by the high computational demands required to adequately model the $A\sim100$ region and its large valence space. Self-Consistent Mean Field (SCMF) DFT calculations, with their global applicability, have also demonstrated promising results in reproducing experimental trends [17, 19–25, 29] and, thus, provide another good option for studying the shape variations in this region.

In spite of the theoretical challenges, within the past few years alone, there has been a multitude of experimen-

* brian.bucher@inl.gov
† Deceased
‡ Present address: Fennovoima Oy, Salmisaarenaukio 1, FI-00180 Helsinki, Finland
§ Present address: TRIUMF, 4004 Wesbrook Mall, Vancouver, BC V6T 2A3, Canada
¶ Present address: Fortum Power Division, P.O. Box 100, FI-00048 Fortum, Finland
** Present address: Cyclotron Institute, Texas A&M University, College Station, Texas 77843, USA
†† Present address: National Superconducting Cyclotron Laboratory, Michigan State University, East Lansing, Michigan 48824 USA
‡‡ Present address: Faculty of Physics, Ludwig-Maximilians University Munich, Am Coulombwall 1, D-85748 Garching, Germany

tal efforts directed towards the $A \sim 100$ region of nuclides [17, 19, 20, 22, 27–36]. Many of the recent experiments have been focused on the sudden increase in deformation for N>60 in isotope chains with Z<40 and how sudden or gradual the isotopic trends are in order to map out the low-Z boundary for which shape coexistence remains prevalent in the low-energy structure [19, 20, 28–31, 37]. Other studies have focused on measuring the collectivity beyond $N = 60$ showing that the maximum in deformation seems to occur at $N = 64$, just ahead of the midshell point [7, 22, 35, 38].

For higher Z ($\geq$42), the evolution of structure and shape coexistence becomes less clear, however it is well known that axial asymmetry begins to play an important role in the low-energy structure [16, 24, 34, 39–47]. Many studies indicate that in Mo and Ru isotopes, the coexisting shapes tend to merge to form relatively rigid, triaxially-deformed ground states [22, 25, 36, 43, 48, 49] or, in the least, potential energy surfaces that are γ-soft [21, 23, 50–52]. The rigidity of triaxial deformation in nuclei remains an open question, but the general consensus is that triaxiality occurs in isotopes that are transitional between two regions where widely different shapes are favored: either between prolate and oblate regions, or between spherical and substantially (quadrupole) deformed regions [14, 21, 24].

However, such an idea about the occurrence of triaxiality and its role in shape-coexisting mass regions may not be complete, especially considering past measurements of shape coexistence in the Z>42 region, particularly in odd-mass isotopes, combined now with the recent experimental and theoretical works mentioned above pertaining to the isotopes at lower Z. Despite the apparent regularity of triaxiality above Mo, shape coexistence does remain an important feature in the low energy structure of Tc [53–56], Rh [44, 57–59], Ag [60], In [61, 62] and to a lesser extent, the even-even isotopes of Ru [63, 64], Pd [65], and Cd [66]. As discussed by Heyde and Wood [11], many have attributed this, perhaps erroneously, to specific, deformation-driving single-particle orbitals crossing the Z=50 shell gap, so-called intruder orbitals. However, an alternative interpretation, with increasing favor recently for the $Z\leq$40 isotopes, suggests that the highly deformed configuration is more due to strong $p - n$ residual interactions that involve a much larger fraction of the valence nucleons [26]. Such interactions have long been considered a key component for a unified description of shape coexistence [67]. Indeed, the minimum in the highly-deformed intruder configuration of Tc [53, 54, 56] and Rh [59] isotopes precisely coincides with the deformation maxima elucidated recently for the lower-Z even-even isotopes Sr [35], Zr [38], and Mo [22] providing an important clue about the evolving structure at higher Z. Up to now, there have been no precise measurements of the collectivity exhibited by these low-lying intruder configurations other than a few lifetimes reported for ^{113,115}Ag in Ref. [60], where little experimental detail was provided, and a couple of uncertain results in ^{109}Rh based on conversion electron [57] and lifetime [59] measurements.

In this manuscript, we report the first precise measurements of collectivity in the higher-Z intruder configuration taken from the isotope $^{109}Rh_{64}$, based on fast timing of excited state lifetimes populated in β decay. In addition, to better understand the interplay between collective and single-particle degrees of freedom exhibited in odd-A nuclides, new calculations based on SCMF theory which properly account for broken symmetries (i.e. axial, time-reversal) and the blocking effect on pairing correlations induced by the odd (unpaired) nucleon [68] are presented. Details related to the experimental work and data analysis are provided in Section II, while the theoretical work is described in Section III. A brief summary and conclusions are provided in Section IV.

II. EXPERIMENT & ANALYSIS

The experimental work was performed at the Ion-Guide Isotope Separator On-Line (IGISOL) facility at the University of Jyväskylä. Isobars with A=109 were produced from induced fission in a thin, natural uranium target by bombarding with 30 MeV protons from a K130 cyclotron. The fission fragments were thermalized in a He gas catcher, extracted and guided into high vacuum with a radiofrequency sextupole device [69], and finally electrostatically accelerated through an isobar separator. More details about the IGISOL technique and facility can be found in Ref. [70].

After mass separation, the A=109 isobars were deposited on an aluminum catcher foil surrounded by scintillation and high-purity germanium (HPGe) detectors to record the β and γ rays emitted as the neutron-rich fission products decayed towards stability. The A=109 isobars were continuously deposited on the catcher foil throughout the data collection period which totaled 33 hours. The average β count rate was 1×10^4 cps. The most neutron-rich A=109 isotope produced from IGISOL in significant quantities was ^{109}Mo, which meant levels and γ rays from all its daughters were observed down to the stable isotope ^{109}Ag. The present report focuses on lifetime measurements made in ^{109}Rh, while measurements from ^{109}Pd, ^{109}Ru, and ^{109}Tc have been reported previously [71, 72].

The new lifetime measurements were obtained using the Advanced Time-Delayed (ATD) $\beta\gamma\gamma(t)$ method [2, 73–75]. In the present experiment, a thin plastic NE111A scintillator was positioned just behind the beam stop to record β rays, while 2 $LaBr_3$(Ce) scintillation detectors were positioned adjacent to (one above and one below) the beam stop at 45° relative to the upstream direction. A HPGe detector of 50% relative efficiency was placed on each side of the beam stop, perpendicular to the beam direction. More details about the experimental setup and subsequent data analysis can be found in Ref. [71].

To obtain level lifetimes, the ATD method uses $\beta\gamma\gamma$

triple coincidences to determine the decay path with β-Ge-Ge coincidences initially examined, taking advantage of the superior energy resolution in those detectors. Then to obtain timing information Ge-β-$LaBr_3$ events are used where the time is recorded through fast electronics; the present case utilized time-to-amplitude converters (TACs) started by β's in the plastic and stopped by γ's in the $LaBr_3$ [71], both having excellent temporal resolution.

For ^{109}Rh, the β-decay scheme of its ^{109}Ru parent is already well-known [57]. The present Ge-Ge coincidence results were consistent with the previous γ-ray and level placements in the relevant low-energy portion (<1 MeV) of the decay scheme where lifetimes could be obtained. The newly measured level lifetimes are summarized in Table I. The lifetimes were primarily obtained by fitting the slopes of the delayed components of the time spectra using the convolution technique [73] where the finite time resolution of the detector pair is accounted for in the fit (Fig. 1a). Note that the high-lying ^{109}Rh states that feed the low-lying levels listed in Table I were checked to ensure those lifetimes were sufficiently short to not affect the measured lifetime values (see Ref. [73] for details). Upper limits on the lifetimes of those states are also listed in Table I. For lifetimes that were too short for the convolution technique, the relative shifts between time-peak centroids from inverted Ge-$LaBr_3$ coincidences were utilized (centroid-shift technique, Fig. 1b) [2, 73], where the time-peak calibration was performed using decay measurements of A=138 isotopes as described in Ref. [71].

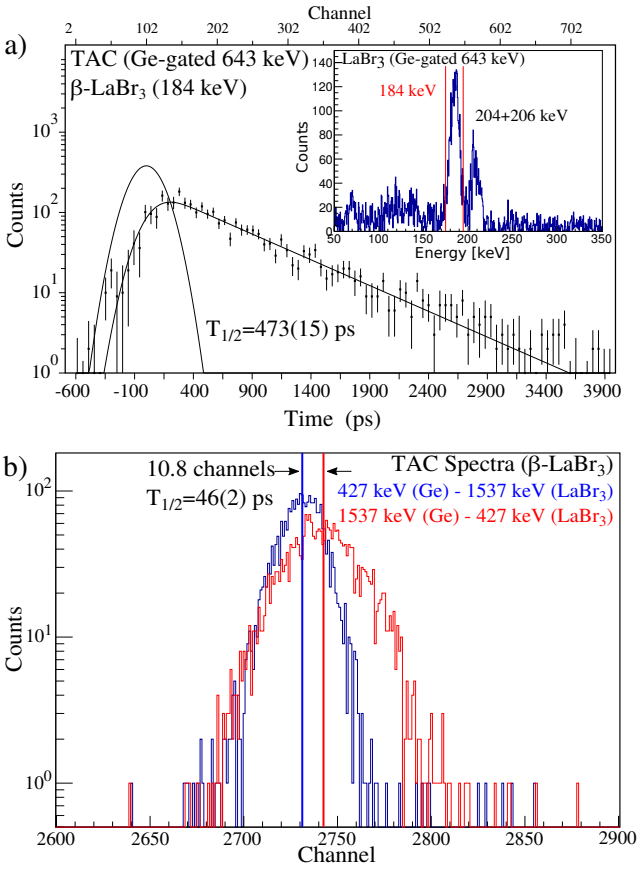

FIG. 1. (Color online) a) The time spectrum (β-$LaBr_3$) obtained by the coincidence gate on the 643.5 keV (Ge) and 183.8 keV ($LaBr_3$) γ rays from the 1053.3 keV and 409.7 keV levels, respectively. The delayed component of the spectrum is due to the lifetime of the 409.7 keV level. The inverted parabola shows the prompt time peak obtained from the fit. The inset shows the corresponding Ge-gated $LaBr_3$ spectrum. b) Time spectra obtained from the coincidence gates on the 426.8 keV and 1537 keV γ rays from the 426.8 keV and 1963 keV levels, respectively. The difference in centroids of the two time peaks, corrected for the energy-dependent time walk and Compton backgrounds (see Ref. [71] for details), is caused by the lifetime of the 426.8 keV level. Note the reduced resolution in $LaBr_3$ at lower energies.

III. RESULTS & DISCUSSION

The new lifetime results include members of the strongly-deformed $K^\pi = 1/2^+$ intruder band up to spin $7/2^+$ along with members of the $K^\pi = 1/2^-$ band originating from the spherical $p_{1/2}$ single-particle orbital and members of the $K^\pi = 7/2^+$ ground-state band originating from the $g_{9/2}$ spherical orbital. Those results with the relevant $M1$ and $E2$ transition probabilities are summarized in Fig. 3. The fast $E2$ transitions in the K^π=$1/2^+$ band with reduced transition probabilites $B(E2; 5/2^+ \rightarrow 1/2^+)$=113(8) W.u. and $B(E2; 7/2^+ \rightarrow 3/2^+)$=136(5) W.u. confirm the enhanced collectivity indicated by previous measurements [57, 59, 60], lending support to the large deformations suggested in prior studies of the nearby isotopes [44, 45, 54, 58]. These $B(E2)$ values are among the largest in the region [79], comparable to those observed in the strongly-deformed bands found in the $Z\leq$42 isotopes [22, 28, 29, 31, 37, 38].

Also of interest are the $E2$ transitions between the $5/2_1^+$ (427 keV) and $9/2_1^+$ (206 keV) levels and the $3/2_2^+$ (359 keV) and $7/2^+$ ground state. The measured $B(E2)$ values suggest that the $5/2_1^+$ and $3/2_2^+$ pair of levels are the anti-aligned component of the γ-vibrational band built on the ground-state quasirotational band (e.g. see Refs. [81, 82]). This is further supported by the similar $M1$ strengths between members of the two pairs (Fig. 3). Another interesting result is the measured $M1$ strength connecting the $3/2^-$ and $5/2^-$ members of the $K^\pi = 1/2^-$ band, which is essentially 1/4 the strength observed in the ground state band supporting the respective $\ell = 1$ and $\ell = 4$ character of the unpaired nucleon in those bands. The $E2$ strength measured in the $K^\pi = 1/2^-$ band between the $5/2^-$ and $1/2^-$ members is consistent with that observed from the $2_1^+ \rightarrow 0_1^+$ transitions in the neighboring even-even ^{108}Ru and ^{110}Pd isotones [83–85]. A lower limit on the $E2$ strength in the ^{109}Rh ground-state band is provided by the very recent measurement of the $11/2_1^+$ (531 keV) lifetime [78] yielding $B(E2)$>12 W.u. for the ground-state transition.

TABLE I. Lifetime results obtained for levels in ^{109}Rh from the present fast timing analysis along with the available literature values. The level energies, spins, and parities were taken from Ref. [77]. Lifetimes reported in Ref. [77] for the levels below are based on prelimary results from a conference presentation of the current measurement and should be superseded by the values reported here. The γ-γ coincidence pairs used in the determination of each lifetime value are listed in the last column (see also Fig. 2).

$E_{\mathrm{Lev.}}$[keV]	J^{π}	$T_{1/2}^{\mathrm{Lit.}}$[ps]	$T_{1/2}^{\mathrm{Pres.}}$[ps]	$\gamma\gamma$ (Ge-$LaBr_3$) [a]
206.2	$9/2^+$	16.7(13)[b]	12(2)[c]	1305-206, 820-206, 466-206, 1078-206
358.6	$3/2^+$	<500[d]	114(2)	68-358, 245-358, 1502-358, 1537-358, 1735-358, 1832-358
409.7	$7/2^+$	430(230)[d]	473(15)	644-184, 226-184
426.8	$5/2^+$	<500[d]	46(2)[c]	1537-427, 1502-427, 245-427
478.3	$(5/2)^+$	<600[d]	166(5)	226-221, 383-221, 383-252, 1616-221, 1616-252
530.7	$11/2^+$	<7.3[b,e]	<90[c]	566-324
568.1	$3/2^-$		<100	226-194
623.1	$5/2^-$		223(10)	116-249
671.9	$(5/2^+)$		<60	358-245, 427-245
740.8	$3/2^-$		<60	116-367, 226-367
856.0	$5/2^-$		<60	249-233, 194-288, 116-288
861.0	$(9/2^+)$		<80	221-383
926.8	$5/2^-$		107(16)	367-186, 194-359
980.7	$(1/2)$		<70	358-622, 367-240, 116-240
1051	$(1/2,3/2,5/2^-)$		<60	116-677
1053	$5/2^+$,$7/2^+$		<60	184-644
1311	$(3/2^+)$		<80	358-266, 358-201
1512	$7/2^+$		<30	206-1305
1576	$5/2^+$,$7/2^+$		<90	358-266, 206-1370
1929	$7/2^+$		<40	206-(1723+1757)[f], 427-(1502+1537)[f]
1963	$(5/2)^+$		<40	206-(1723+1757)[f], 427-(1502+1537)[f]
2094	$(3/2^+)$		<40	116-1720
2190	$(3/2^+)$		<40	358-1832

[a] Inverted gates included for centroid-shift results
[b] Ref. [78], published during the final editing stages of this manuscript
[c] Centroid-shift technique
[d] Ref. [59]
[e] 95% confidence
[f] Unresolved in $LaBr_3$

In an attempt to better understand the mechanisms behind shape coexistence, triaxiality, and their interplay with single-particle degrees of freedom, a novel SCMF calculation with proper treatment of the odd, unpaired nucleon has been performed. The novelty resides on the $\langle \hat{J}_z^2 \rangle$ constraint (as discussed below) used to identify the configurations of interest. For a recent comparison of state of the art Hartree-Fock-Bogoliubov (HFB) blocking calculations with different interactions, relativistic and nonrelativistic, see Ref. [86]. In the past, only simplistic particle-rotor calculations were performed to study odd-A isotopes in the higher-Z Rh region, with parameters derived empirically to match experimental observations [44, 45, 53, 54]. Such calculations provided some characterization of the shape coexistence and triaxiality in these odd-A systems, but could not say anything regarding the underlying microscopic structure responsible for these phenomena. The calculations here are based on the HFB method with the Gogny D1S interaction. To begin, a "reference" calculation of the β-γ potential energy surface (PES) is performed. In this "reference" calculation ^{109}Rh is treated as an even-even nucleus (i.e. time-odd fields are set to zero) but with the appropriate constraints that $\langle Z \rangle = 45$ and $\langle N \rangle = 64$. In the β-γ PES obtained in this way and depicted in Fig. 4, a triaxial minimum is observed at $Q_0 = 4$b, where $\beta = \sqrt{4\pi/5} Q_0/(A\langle r^2 \rangle)$, and $\gamma \approx 25^\circ$ as well as prolate and oblate saddle points at $Q_0 = 4$b, $\gamma = 0^\circ$ and $Q_0 = 3$b, $\gamma = 60^\circ$, respectively.

In order to properly describe the structure of odd-A nuclides, specific wave functions tailored to deal with the odd number of particles are required. They are obtained by the blocking procedure [87], which breaks time-reversal invariance and generates time-odd fields. Taking one of the "reference" wave functions with a given value of Q_0 and γ, we block a proton quasiparticle state and look for the self-consistent blocked solution using the gra-

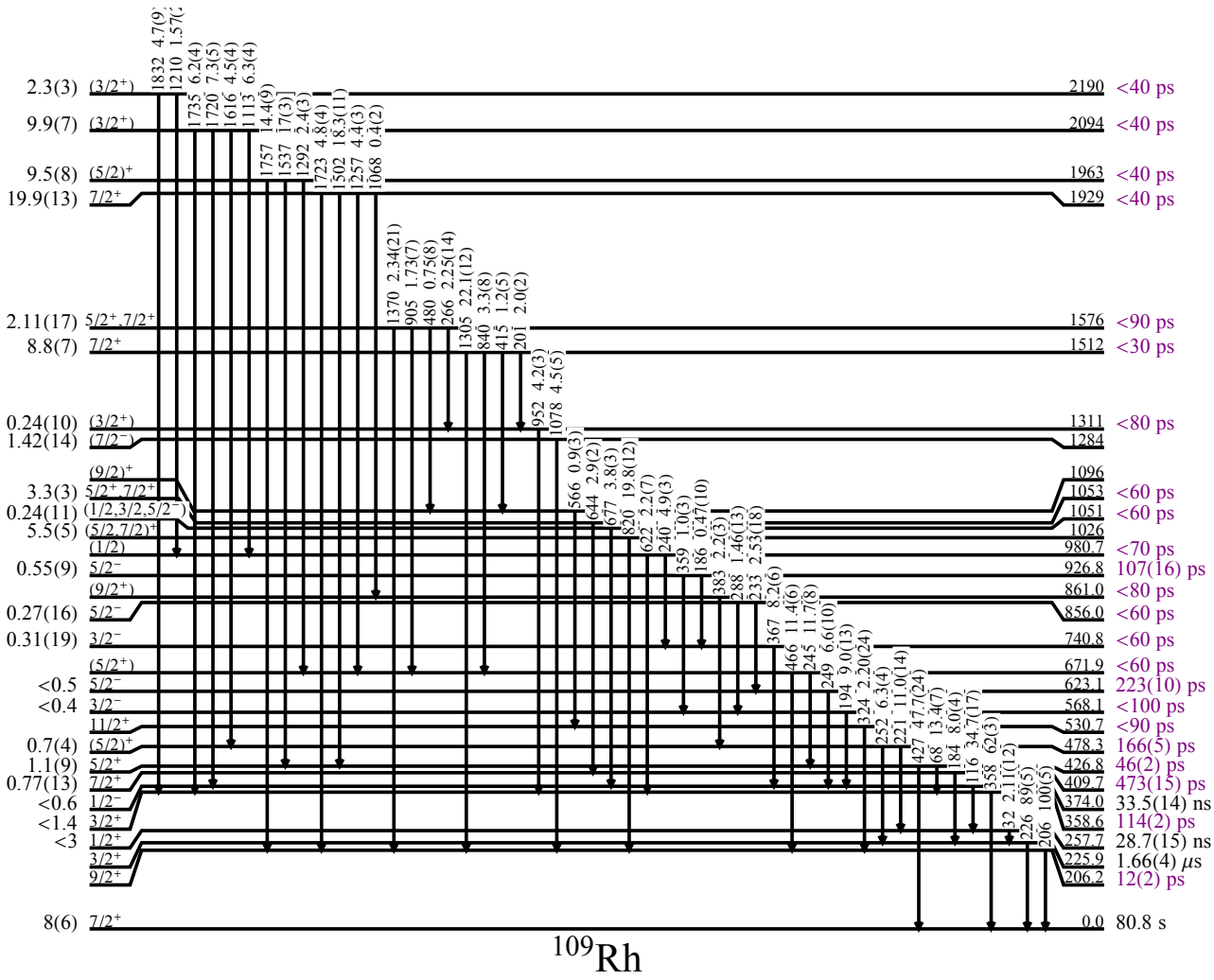

FIG. 2. (Color online) A partial β-decay scheme showing the relevant levels and γ rays used for the timing analysis and results presented in Table I. The β-feeding intensities from Refs. [57, 77] are provided on the left along with the relative γ-ray intensities displayed above each transition. Lifetimes obtained from the present work are labeled in purple font.

dient method [88]. This procedure is repeated for a few of the lowest lying proton quasiparticle excitations. The blocked solution with the lowest energy is the ground state and other solutions correspond to excited states. Although all self-consistent symmetries are preserved in the calculation, in the present case the only one that breaks degeneracies is parity, so the number of states to be obtained is limited to two. The positive-parity blocked state turns out to have a $\langle J_z^2 \rangle$ value equivalent to $K = 7/2^+$ (K is not a good quantum number for triaxial wave functions). The negative-parity state lies at an excitation energy of 0.869 MeV and its $\langle J_z^2 \rangle$ value is equivalent to $K = 1/2^-$. The excitation energy of the $K = 1/2^-$ is a factor of two too high but this is not so crucial given the global character of the Gogny D1S parameter set. Another successful Gogny parametrization, D1M, reduces the excitation energy to 0.667 MeV. The β deformation parameter of both states is rather similar while the γ values differ slightly—see Table II. The experimental ground-state spin and parity are well-reproduced in this triaxial calculation and cannot be obtained in an axially-symmetric calculation. This is seen in the middle panel of Fig. 4 where the single-particle energies (SPE) are obtained by diagonalizing the HF hamiltonian. The plots show the evolution of the SPE as a function of the deformation parameter Q_0 on both the prolate (left) and oblate (right) sides, ending at a deformation $Q_0 = 3.8$b which corresponds to the prolate axial saddle point. They are connected by a plot showing the behavior of the SPE as a function of the γ deformation parameter with Q_0 fixed at 3.8b. The position of the proton Fermi level is marked by a dotted red line. In the spherical configuration the proton $g_{9/2}$ orbital is at the Fermi level. The $K = 7/2^+$ orbital is above the Fermi level in the prolate side whereas the $K = 5/2^+$ remains below. On the other hand, the $K = 1/2^-$ orbital originating from $p_{1/2}$ quickly approaches the Fermi level. Therefore it is not surprising that a full self-consistent blocking calculation preserv-

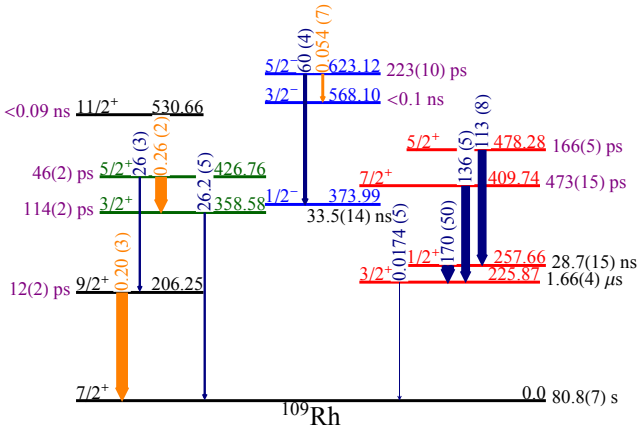

FIG. 3. (Color) Low-lying levels and transitions in ^{109}Rh. New lifetimes are labeled in purple; the others were taken from Ref. [77]. Transition multipolarities are assumed pure unless experimental data exists to indicate otherwise [80]. $E2$ transitions are labeled dark blue, while $M1$ transitions are orange. The $B(X\lambda)$ probabilities are labeled above in Weisskopf units. The level colors indicate the various band structures: ground-state (black), $K = 1/2^+$ (red), $K = 1/2^-$ (blue), and γ-band (green), see text for details. Note that for ease of viewing not all transitions have been displayed.

ing axial symmetry yields the ordering $1/2^-$, $5/2^+$, $1/2^+$ (this one having a larger Q_0 value) and $7/2^+$ for the prolate excited states. In this axial calculation the ground state is actually oblate and the level ordering in that well is $3/2^+$, $1/2^+$ and $5/2^+$. In order to reproduce the experimental ground state spin and parity $J^\pi = 7/2^+$ one needs to go to the triaxial sector in order to mix the $7/2^+$ with other orbitals to bring it closer to the Fermi level (at $\gamma = 30°$).

In order to obtain other excited states we have carried out blocked calculations constraining the value of $\langle J_z^2\rangle$ - $\langle J_z^2\rangle_{\rm ref}$, where the latter is the $\langle J_z^2\rangle$ value of the "reference" calculation. By constraining the quantity to 0.25 we obtain results for the $K = 1/2^+$ band head. The corresponding β and γ deformation parameters are given in Table II. We observe how the β parameter of the $K = 1/2^+$ is larger than the one of the ground state while the γ parameter is smaller. This difference in deformation parameters naturally explains the slow $E2$ transition between the $J^\pi = 3/2^+$, built on the $K = 1/2^+$ band head, and the ground state. Moreover, the ratio of β deformations between the positive- and negative-parity $K = 1/2$ bands is consistent with the experimental ratio of deformations obtained from the measured $B(E2)$ values and rotational approximation (within $0.3\,\sigma$). An interesting feature of the calculation is the structure of the energy landscape for the different blocked quasiparticles. On the right side of Fig 4, the minimum value of energy $E(\beta,\gamma)$ is plotted as a function of β for each blocking configuration. The minima of the $K = 7/2^+$ and $K = 1/2^-$ have nearly the same deformation but much different than the shape isomeric $K = 1/2^+$, as

TABLE II. The energies and deformations calculated for the lowest few blocked quasiparticle configurations. The $K^\pi = 1/2^+$ calculation requires a constraint on $\langle J_z^2\rangle$.

K^π	$E_{\rm exc}$ (keV)	β	γ
$7/2^+$	0	0.26	26°
$1/2^+$	567	0.33	16°
$1/2^-$	869	0.25	14°

described above. The topologies of the three curves are quite distinct reflecting the unique response of the system to dynamical fluctuations in the Q_0 degree of freedom. The main outcome is that different blocked configurations have different PESs each with minima located at unique values of deformation having correspondingly unique shapes. The position and depth of those minima can give us clues about the structure of the corresponding physical states, however the global character of Gogny D1S does not allow for a spectroscopic-quality description of those states. An example of this deficiency, characteristic of all relativistic and nonrelativistic functionals, is discussed at length in Ref. [86] where blocking HFB calculations were carried out in a series of superheavy nuclei. As discussed there, the systematic discrepancies can be expected across the whole periodic table. In that study it was found that although the relative ordering of levels was usually not reproduced, all the low-lying states observed experimentally were also present in the calculations.

IV. SUMMARY & CONCLUSIONS

To summarize, sub-nanosecond lifetimes of excited states in the odd-Z isotope ^{109}Rh were measured via fast electronic timing. These results provide new insight into the shape coexistence present in the neutron-rich mass region above A=100 and confirm the persistence there of similarly enhanced quadrupole deformations observed near Z∼40, N∼60. In addition, a novel SCMF calculation tailored for odd-mass nuclei in this mass region, based on the HFB method with Gogny D1S interaction and properly accounting for associated axial and time-reversal asymmetries, has been carried out. The calculations confirm the importance of ground-state triaxiality in this region, as previously indicated by more simplistic particle-rotor models, yet reproducing the experimentally-observed shape coexistence in a self-consistent way. The new calculations highlight the intimate role that the unpaired nucleon plays in picking different shapes based on the single-particle level occupied. This has a blocking effect on the pairing correlations that tend to mix various shapes in the even-even isotopes, explaining the more pronounced shape coexistence observed in the odd-A isotopes of this mass region. From a microscopic point of view, triaxial shapes be-

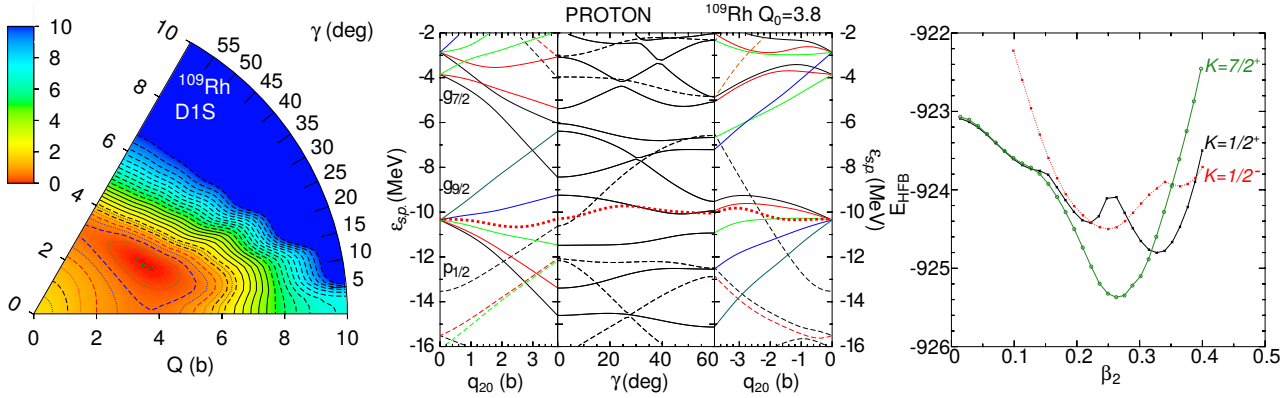

FIG. 4. (Color) Left: The calculated β-γ potential energy surface for ^{109}Rh. Middle: The proton single-particle energies as a function of deformation parameters Q_0 and γ. The left (right) side has γ fixed at 0° (60°) corresponding to a prolate (oblate) axial shape. The center panel shows the variation as a function of γ with Q_0 fixed at 3.8b. Right: The minimum energy $E(\beta,\gamma)$ for the different blocked configurations.

come favorable here, where large quadrupole deformation is reinforced by strong $p-n$ interactions between highly-overlapping orbitals (i.e. $\pi g_{9/2}$ and $\nu g_{7/2}$), as the Fermi surface approaches the higher-lying K components. This enables a large gain in binding energy to occur through the mixing of high- and low-K orbitals.

ACKNOWLEDGMENTS

The authors acknowledge helpful discussions with C.Y. Wu (LLNL). Figures 2 & 3 were created using the *LevelScheme* scientific figure preparation system [89]. This project was funded by the National Science Foundation through grants PHY0822648, PHY0758100, and PHY1419765 and supported by EU 6$^{\text{th}}$ Framework program (Integrating Infrastructure Initiative—Transnational Access) contract number: 506065 (EURONS), the U.S. Department of Energy under Contract No. DE-AC07-05ID14517, the Spanish MINECO via FPA-2015-65035-P, and by the Academy of Finland under the Centre of Excellence Programme 2006-2011 (nuclear and accelerator based physics program at JYFL). The work of LMR was partly supported by Spanish MINECO grant Nos. FPA2015-65929 and FIS2015-63770.

[1] P. Federman, S. Pittel, and A. Etchegoyen, Phys. Lett. B **140**, 269 (1984).
[2] H. Mach *et al.*, Nucl. Phys. A **523**, 197 (1991).
[3] T. Kautzsch *et al.*, Eur. Phys. J. A **9**, 201 (2000).
[4] M. Bender, P.-H. Heenen, and P.-G. Reinhard, Rev. Mod. Phys. **75**, 121 (2003).
[5] T. Otsuka *et al.*, Phys. Rev. Lett. **95**, 232502 (2005).
[6] T. Otsuka *et al.*, Phys. Rev. Lett. **104**, 012501 (2010).
[7] T. Sumikama *et al.*, Phys. Rev. Lett. **106**, 202501 (2011).
[8] H. Watanabe *et al.*, Phys. Rev. Lett. **113**, 042502 (2014).
[9] P. Federman and S. Pittel, Phys. Rev. C **20**, 820 (1979).
[10] N. A. Smirnova *et al.*, Phys. Lett. B **686**, 109 (2010).
[11] K. Heyde and J. L. Wood, Rev. Mod. Phys. **83**, 1467 (2011).
[12] D. Bonatsos *et al.*, Phys. Rev. C **88**, 054309 (2013).
[13] J. H. Hamilton *et al.*, J. Phys. G **10**, L87 (1984).
[14] A. G. Smith *et al.*, Phys. Rev. C **86**, 014321 (2012).
[15] A. Kankainen, J. Äystö, and A. Jokinen, J. Phys. G **39**, 093101 (2012).
[16] A. Görgen and W. Korten, J. Phys. G **43**, 024002 (2016).
[17] A. de Roubin *et al.*, Phys. Rev. C **96**, 014310 (2017).
[18] B. Cheal *et al.*, Phys. Rev. Lett. **102**, 222501 (2009); F. C. Charlwood *et al.*, Phys. Lett. B **674**, 23 (2009); B. Cheal *et al.*, Phys. Lett. B **645**, 133 (2007).
[19] F. Flavigny *et al.*, Phys. Rev. Lett. **118**, 242501 (2017).
[20] S. Chen *et al.*, Phys. Rev. C **95**, 041302(R) (2017).
[21] H. Abusara, S. Ahmad, and S. Othman, Phys. Rev. C **95**, 054302 (2017).
[22] D. Ralet *et al.*, Phys. Rev. C **95**, 034320 (2017).
[23] K. Nomura, R. Rodríguez-Guzmán, and L. M. Robledo, Phys. Rev. C **94**, 044314 (2016).
[24] J. Xiang *et al.*, Phys. Rev. C **93**, 054324 (2016).
[25] C. L. Zhang *et al.*, Phys. Rev. C **92**, 034307 (2015).
[26] T. Togashi *et al.*, Phys. Rev. Lett. **117**, 172502 (2016).
[27] C. Kremer *et al.*, Phys. Rev. Lett. **117**, 172503 (2016).
[28] J.-M. Régis *et al.*, Phys. Rev. C **95**, 054319 (2017).
[29] E. Clément *et al.*, Phys. Rev. Lett. **116**, 022701 (2016).
[30] J. Dudouet *et al.*, Phys. Rev. Lett. **118**, 162501 (2017).
[31] T. W. Hagen *et al.*, Phys. Rev. C **95**, 034302 (2017).
[32] A. E. Stuchbery, S. K. Chamoli, and T. Kibédi, Phys. Rev. C **93**, 031302(R) (2016).
[33] M. Rejmund *et al.*, Phys. Lett. B **753**, 86 (2016).
[34] A. Navin *et al.*, Phys. Lett. B **767**, 480 (2017).
[35] J. Park *et al.*, Phys. Rev. C **93**, 014315 (2016).
[36] D. T. Doherty *et al.*, Phys. Lett. B **766**, 334 (2017).
[37] C. Sotty *et al.*, Phys. Rev. Lett. **115**, 172501 (2015).
[38] F. Browne *et al.*, Phys. Lett. B **750**, 448 (2015).
[39] C. Liu *et al.*, Phys. Rev. C **88**, 037301 (2013).

[40] S. Lalkovski *et al.*, Phys. Rev. C **88**, 024302 (2013).
[41] S. H. Liu *et al.*, Phys. Rev. C **84**, 014304 (2011).
[42] J. Pinston *et al.*, Phys. Rev. C **74**, 064304 (2006).
[43] P. Möller *et al.*, Phys. Rev. Lett. **97**, 162502 (2006).
[44] Y. X. Luo *et al.*, Phys. Rev. C **69**, 024315 (2004).
[45] Ts. Venkova *et al.*, Eur. Phys. J. A **6**, 405 (1999).
[46] Ts. Venkova *et al.*, Eur. Phys. J. A **15**, 429 (2002).
[47] J. H. Hamilton *et al.*, Nucl. Phys. A **834**, 28c (2010).
[48] Y. X. Luo *et al.*, Phys. Lett. B **670**, 307 (2009).
[49] M. Varshney *et al.*, Phys. Scr. **83**, 015201 (2011).
[50] S. Lalkovski *et al.*, Eur. Phys. J. A **18**, 589 (2003).
[51] B. Sorgunlu and P. Van Isacker, Nucl. Phys. A **808**, 27 (2008).
[52] E. A. Stefanova *et al.*, Phys. Rev. C **86**, 044302 (2012).
[53] Y. X. Luo *et al.*, Phys. Rev. C **70**, 044310 (2004).
[54] G. Simpson *et al.*, Phys. Rev. C **75**, 027301 (2007).
[55] A. M. Bruce *et al.*, Phys. Rev. C **82**, 044312 (2010).
[56] J. Kurpeta *et al.*, Phys. Rev. C **86**, 044306 (2012).
[57] N. Kaffrell *et al.*, Nucl. Phys. A **470**, 141 (1987).
[58] J. Rogowski *et al.*, Phys. Lett. B **207**, 125 (1988).
[59] G. Lhersonneau *et al.*, Eur. Phys. J. A **1**, 285 (1998).
[60] J. Rogowski *et al.*, Phys. Rev. C **42**, 2733 (1990).
[61] W. Dietrich *et al.*, Nucl. Phys. A **253**, 429 (1975).
[62] R. Lucas *et al.*, Eur. Phys. J. A **15**, 315 (2002).
[63] J. Stachel *et al.*, Nucl. Phys. A **383**, 429 (1982).
[64] J. C. Wang *et al.*, Phys. Rev. C **61**, 044308 (2000).
[65] G. Lhersonneau *et al.*, Eur. Phys. J. A **2**, 25 (1998).
[66] S. Juutinen *et al.*, Phys. Lett. B **386**, 80 (1996).
[67] K. Heyde *et al.*, Phys. Rep. **102**, 291 (1983).
[68] S. Wahlborn, Nucl. Phys. **37**, 554 (1962).
[69] P. Karvonen *et al.*, Nucl. Instrum. Methods B **266**, 4794 (2008).
[70] I. D. Moore, P. Dendooven, and J. Ärje, Hyperfine Interact. **223**, 17 (2014).
[71] B. Bucher *et al.*, Phys. Rev. C **92**, 064312 (2015).
[72] M. K. Smith, Ph.D. thesis, University of Notre Dame (2017).
[73] H. Mach, R. L. Gill, and M. Moszyński, Nucl. Instrum. Methods **A280**, 49 (1989).
[74] M. Moszyński and H. Mach, Nucl. Instrum. Methods **A277**, 407 (1989).
[75] H. Mach and L. M. Fraile, Hyperfine Interact. **223**, 147 (2014).
[76] See Supplemental Material at [URL TBD].
[77] S. Kumar, J. Chen, and F. G. Kondev, Nucl. Data Sheets **137**, 1 (2016).
[78] T. W. Hagen *et al.*, Eur. Phys. J. A **54**, 50 (2018).
[79] B. Pritychenko *et al.*, At. Data Nucl. Data Tables **107**, 1 (2016).
[80] In the most recent evaluation [77], the level at 258 keV was assigned a spin of (3/2) based on an experimental $\alpha(K)$ of the 221 keV transition from the $(5/2)^+$ level above at 478 keV reported in Ref. [90]. However, the reported value is consistent with a pure $E2$ transition multipolarity within 1σ and the level systematics presented in Ref. [59] indicate the spin should be 1/2 for this level.
[81] G. Gervais *et al.*, Nucl. Phys. A **624**, 257 (1997).
[82] J. Iwanicki *et al.*, J. Phys. G **29**, 743 (2003).
[83] J. Blachot, Nucl. Data Sheets **91**, 135 (2000).
[84] G. Gürdal and F. G. Kondev, Nucl. Data Sheets **113**, 1315 (2012).
[85] Brookhaven National Laboratory, "NNDC Nuclear Database," `http://www.nndc.bnl.gov/`, (Accessed October 2017).
[86] J. Dobaczewski *et al.*, Nucl. Phys. A **944**, 388 (2015).
[87] P. Ring and P. Schuck, *The Nuclear Many-Body Problem* (Springer-Verlag Berlin Heidelberg, 1980).
[88] L. M. Robledo, R. Bernard, and G. F. Bertsch, Phys. Rev. C **86**, 064313 (2012).
[89] M. A. Caprio, Comput. Phys. Commun. **171**, 107 (2005), `http://scidraw.nd.edu/levelscheme`.
[90] H. Penttilä, Ph.D. thesis, University of Jyväskylä (1992).